Robotica (2012) volume 30, pp. 1029–1039. © Cambridge University Press 2012
doi:10.1017/S0263574711001329

# Calibration of wheeled mobile robots with differential drive mechanisms: an experimental approach

Y. Maddahi†, N. Sepehri†,*, A. Maddahi‡ and M. Abdolmohammadi§

†*Department of Mechanical and Manufacturing Engineering, University of Manitoba, Winnipeg, Canada*
‡*Department of Mechanical Engineering, K. N. Toosi University of Technology, Tehran, Iran*
§*School of Manufacturing Engineering, Science and Research Division, Islamic Azad University, Tehran, Iran*

(Accepted December 3, 2011. First published online: January 12, 2012)

**SUMMARY**

Exact knowledge of the position and proper calibration of robots that move by wheels form an important foundation in mobile robot applications. In this context, a variety of sensory systems and techniques have been developed for accurate positioning of differential drive mobile robots. This paper, first, provides a brief overview of mobile robots positioning techniques and then, presents a new benchmark method capable of calibrating mobile robots with differential drive mechanisms to correct systematic errors. The proposed method is compared with the commonly used University of Michigan Benchmark (UMBmark) odometry method. Two sets of comparisons are conducted on six prototyped robots with differential drives. The first set of tests establishes the workability and accuracy that can be achieved with the new method and compares them with the ones obtained from the UMBmark technique. The second experiment compares the performance of a mobile robot, calibrated with either the UMBmark or the new method, for an unseen path. It is demonstrated that the proposed method of calibration is simple to implement, and leads to accuracy comparable to the UMBmark method. Specifically, while the error corrections in both methods are within $\pm 5\%$ of each other, the proposed method requires single straight line motion for calibration, which is believed to be simpler and less timely to implement than the square path motion required by the UMBmark technique. The method should therefore be considered seriously as a new tool when calibrating differential drive mobile robots.

KEYWORDS: Differential drive mobile robots; Systematic error; Benchmark tests; Error improvement; Performance analysis; Statistical results.

## 1. Introduction

Calibration is defined as a set of operations that establishes, under specified conditions, relationship between the values of quantities indicated by a measuring instrument and the corresponding values realized by standards.[1] Calibration is used to correct both systematic and nonsystematic errors. Systematic errors are caused by imperfections during design, fabrication, and assembly. Nonsystematic errors, on the other hand, are unwanted errors created during the robot motion. Recently, there have been many efforts to develop effective calibration methods for robotic systems.[2] They include odometry,[3] 3D camera error detection,[4] active beacons,[5] gyroscope,[6] and magnetic compasses.[7] Odometry is the use of data from the movement of actuators to estimate change in position over time. As compared to other methods, odometry provides better short-term accuracy allowing very high sampling rates with lower costs.[8] Using the odometry technique, fewer landmarks (stationary signs placed in between start and stop points) are needed for certain length of robot trajectory.[8] The odometry method can be applied to correct errors of all types of mobile robots including vehicle-type robots and robots with differential drives. Odometry calibration can be conducted offline or online. Offline odometry calibration is mostly used by defining an expanded mobile robot kinematics model and corresponding calibration parameters.[9,10] Offline calibration allows initial calibration to correct robot positioning errors, followed by further online calibration using high-accuracy instruments.[11] This paper focuses on offline odometry calibration as the first step of the calibration process.

Effective application of odometry approach in robot calibration has been a research goal in mobile robotics for many years.[12–17] The most notable one is the work done by Borenstein and Feng[18–20] who introduced a method for measuring odometry errors in differential drive mobile robots, which they named University of Michigan Benchmark (UMBmark) method. They implemented this method to correct errors for a number of robots including differential drive and omnimate mobile robots. In a different study, Maddahi *et al.*[21] applied the UMBmark test on different types of differential drive mobile robots to correct systematic positioning errors[22] and extended UMBmark test for nonsystematic positioning errors.[23] The results confirmed the significance and effectiveness of odometry method in the process of mobile robot calibration. This paper presents new results of experimental evaluation of the widely used UMBMark odometry method for calibration of differential drive mobile robots and further proposes an alternative method. The proposed method is simple to implement, and because it is built upon kinematics, it is applicable to all types of wheeled mobile robots including differential drive, omnidirectional, and high degrees of freedom wheeled mobile robots. The proposed method is experimentally

* Corresponding author. E-mail: nariman@cc.umanitoba.ca

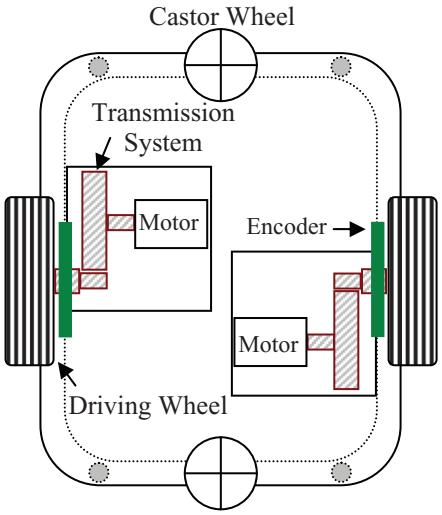


Fig. 1. (Colour online) Main components of differential drive mobile robot.

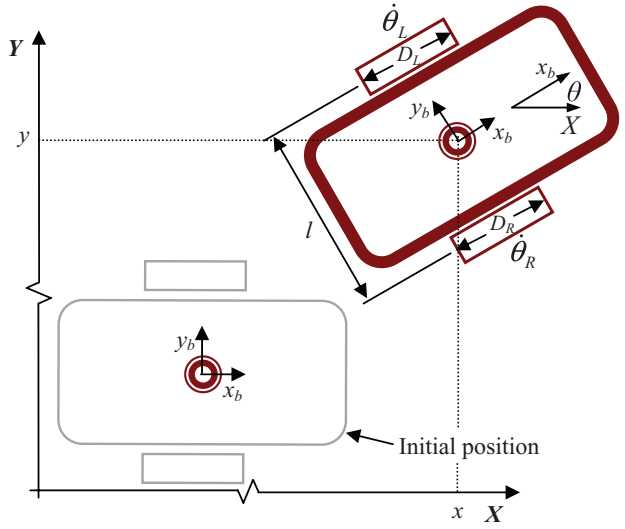


Fig. 2. (Colour online) Coordinate frames and parameters of wheeled mobile robot.

shown to produce position accuracy and percentage of error reduction, comparable to the UMBmark approach when applied to differential drive robots.

The robots used in this paper are all prototyped in-house, for various purposes and use differential mechanisms. The characteristics and kinematics modeling of differential drive robots are briefly presented in Section 2. Section 3 briefly outlines the formulation of the UMBmark, followed by detailed description of the proposed method in Section 4. The implementation of both methods is addressed in Section 5. Section 6 describes the prototyped mobile robots. Experimental results, comparing the performance of both calibration approaches as applied to all six types of mobile robots, are given in Section 7 followed by presenting some statistical analyses on the basis of experimental data obtained using both the methods. Conclusions are provided in Section 8.

## 2. Brief Background on Differential Drive Mobile Robots

Figure 1 shows the structure of a typical differential drive mobile robot. The two driving wheels are actively controlled to move the robot in various directions. Castor wheels are used to maintain balance.

With reference to Fig. 2, the kinematics equations of differential drive robots are obtained using Denavit–Hartenberg notation.[24] On the basis of these equations, the mobile robot is subject to three constraints. The first two constraint equations are derived from the fact that two driving wheels roll and do not slip[25]:

$$\dot{x}\cos\theta + \dot{y}\sin\theta = (D_L\dot{\theta}_L + D_R\dot{\theta}_R)/4, \tag{1}$$

$$\dot{\theta} = (D_R\dot{\theta}_R - D_L\dot{\theta}_L)/2l. \tag{2}$$

The third equation relates to the fact that the mobile robot cannot move in the lateral direction defined as[25]

$$\dot{x}\sin\theta - \dot{y}\cos\theta = 0. \tag{3}$$

With reference to Fig. 2, $l$ denotes the nominal distance between the two driving wheels. $x$ and $y$ are the coordinates of the base (body attached) coordinate frame $\{x_b y_b\}$ with respect to the fixed (global) coordinate system $\{XY\}$. $\theta$ represents the orientation of the robot, which is the angle between the base frame $\{x_b y_b\}$ and the fixed frame $\{XY\}$. $D_R$ and $D_L$ denote nominal diameters of right and left wheels, respectively.

## 3. UMBmark Method

The UMBmark method is based on compensating two dominant error sources. The first one is caused by the unequal wheel diameters ($D_R$ and $D_L$) and the second one relates to the uncertainty on the value of the wheelbase, $l$ (see Fig. 2). Using UMBmark method, the robot starts out at a "start" position and moves along a 4 m × 4 m unidirectional square path in clockwise (CW) and/or counterclockwise (CCW) directions. The robot is programmed to travel along all four legs of the square path. However, because of the odometry errors, it will likely not arrive precisely at the start position, $O$. Figure 3 illustrates the schematic of expected experimental results in CCW direction. In addition, it depicts the desired (solid line) and actual (dashed line) trajectories obtained during robot motion. Also, the contribution of two types of error labeled with $\alpha$ and $\beta$ angles can be seen in this figure.

Upon completion of each trial, the position offsets along $x$ and $y$ axes ($\delta x_i^{\mathrm{CW/CCW}}$ and $\delta y_i^{\mathrm{CW/CCW}}$) are measured with respect to the start point (see Fig. 3). Mean position errors are then calculated using the following equations[20]:

$$\delta x^{\mathrm{CW/CCW}} = \frac{1}{n}\sum_{i=1}^{n}\delta x_i^{\mathrm{CW/CCW}}, \tag{4}$$

$$\delta y^{\mathrm{CW/CCW}} = \frac{1}{n}\sum_{i=1}^{n}\delta y_i^{\mathrm{CW/CCW}}, \tag{5}$$

where $n$ is the number of test runs.

https://doi.org/10.1017/S0263574711001329 Published online by Cambridge University Press

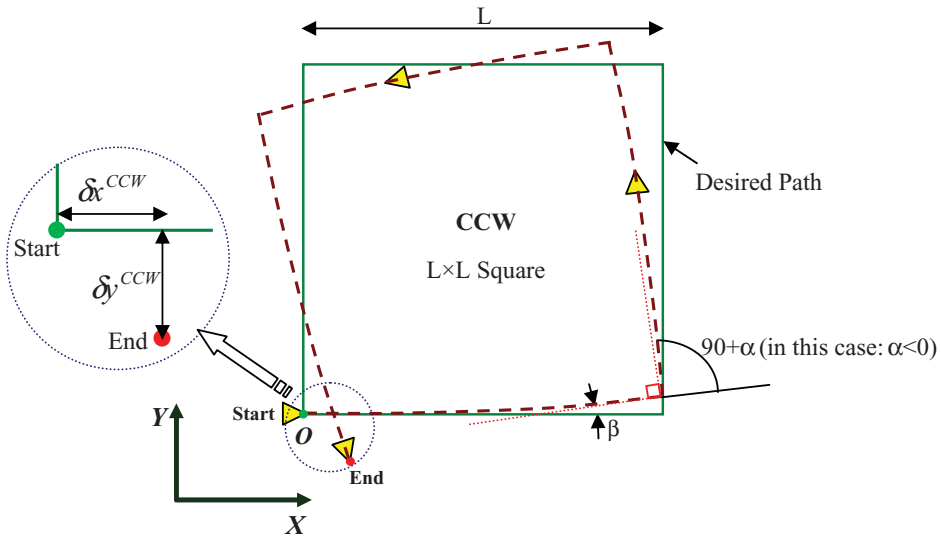


Fig. 3. (Colour online) UMBmark test path in CCW direction. Uncertainty about the wheelbase causes the robot to turn $(90 + \alpha)$ degrees, instead of the desired 90 degrees. Difference in the wheel diameters moves it along dashed lines, instead of the desired straight lines contributing to formation of nonzero angle $\beta$.

Based on the calculated position offsets, the coefficients $\alpha$ and $\beta$ are found from simple geometric relations. Note that $\alpha$ and $\beta$ can be positive or negative depending on the ratio of wheel diameters, actual wheelbase, and the actual position of robot[20]

$$\alpha = \left(\frac{\delta x^{CW} + \delta x^{CCW}}{-4L}\right)\left(\frac{180}{\pi}\right) = \left(\frac{\delta y^{CW} - \delta y^{CCW}}{-4L}\right) \times \left(\frac{180}{\pi}\right), \tag{6}$$

$$\beta = \left(\frac{\delta x^{CW} - \delta x^{CCW}}{-4L}\right)\left(\frac{180}{\pi}\right) = \left(\frac{\delta y^{CW} + \delta y^{CCW}}{-4L}\right) \times \left(\frac{180}{\pi}\right). \tag{7}$$

In Eqs. (6) and (7), $L$ is the straight leg of the square path. Using the coefficients $\alpha$ and $\beta$, the values of $E_b$ and $E_d$ are calculated as follows:

$$E_b = \frac{\hat{l}}{l} = \frac{90^\circ}{90^\circ - \alpha}, \tag{8}$$

$$E_d = \frac{\hat{D}_R}{\hat{D}_L} = \frac{D_R}{D_L}\frac{L + l\sin\left(\beta/2\right)}{L - l\sin\left(\beta/2\right)}. \tag{9}$$

The superscript "^" indicates actual value of the parameter. The actual wheelbase $(\hat{l})$ is redefined in software according to Eq. (8) in terms of $E_b$ and nominal wheelbase $(l)$, based on the initial measurement. The correction for the unequal wheel diameters, based on factor $E_d$, is slightly more involved. After performing the test procedure, the actual wheel diameter ratio $(\hat{D}_R/\hat{D}_L)$ from Eq. (9) is calculated. However, when applying a compensation factor, we should make sure not to change the average wheel diameter,[20] i.e., $D_R + D_L = \hat{D}_R + \hat{D}_L$. Using the average wheel diameter and Eq. (9), the actual values of right and left wheel diameters can be obtained.

## 4. Proposed Method

The UMBmark method is capable of producing reliable and reasonable results for differential drive mobile robots. The method, however, is built upon the consideration that positioning errors are mainly due to unequal diameters of the two wheels and uncertainty on the distance between the two wheels (wheelbase length). The method, therefore, cannot correct the errors in mobile robots of other types, such as mobile robots with more than two driving wheels. Lack of a simple, yet reliable method capable of calibrating errors in all types of wheeled mobile robots considering all system errors has motivated the authors to propose a new approach.

The proposed method is built upon kinematic Eqs. (1)–(3) and aims at improving "lateral" and "longitudinal" errors. Figure 4 shows the defined trajectory and related variables. With reference to Fig. 4, the robot is directed to move along the desired straight line (path A) in Cartesian coordinates $\{XY\}$. Due to systematic errors, regardless of the sources, the robot follows a different path (path B). Using Eq. (2) and assuming the constant linear velocity for robot over the test period, the mobile platform orientation error $(\lambda)$ is expressed as follows:

$$\lambda = \left(\frac{1}{4l}\right)(D_R\theta_R - D_L\theta_L). \tag{10}$$

In Eq. (10), $\theta_R$ and $\theta_L$ are the total orientation of right and left wheels, respectively.

In order to reduce position error, the robot must be kept along the desired trajectory (path A) by reorienting itself continuously during the motion. Thus, a new coefficient, named "lateral corrective factor" $(F_{\text{lat}})$, is defined which presents the ratio of the wheels angular velocities. This coefficient is used to calculate the modified angular

https://doi.org/10.1017/S0263574711001329 Published online by Cambridge University Press

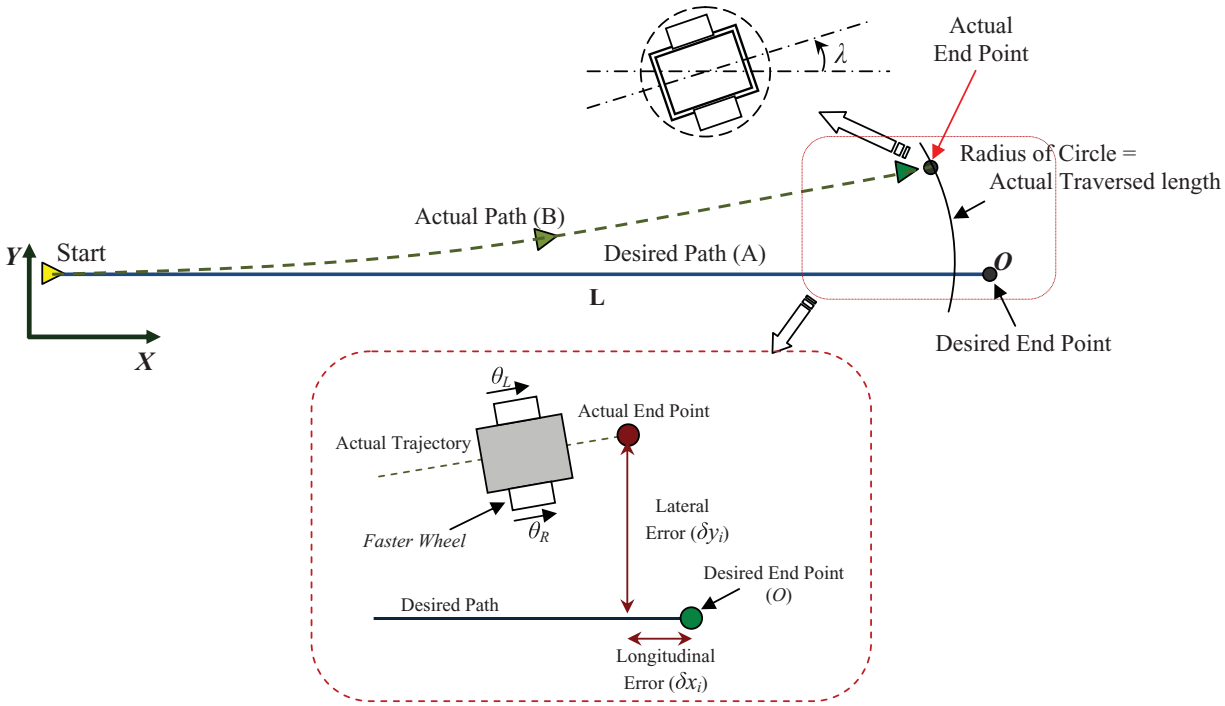


Fig. 4. (Colour online) Trajectories in the proposed method: desired path (A) actual path (B). The actual position is measured with respect to the desired end point $O$.

displacements (and subsequently velocities) in order to achieve the perfect movement along the straight trajectory

$$F_{\text{lat}} = \theta_R/\theta_L. \tag{11}$$

From Eq. (11), $F_{\text{lat}} > 1$ implies the right wheel must rotate faster than the left one. Combining Eqs. (10) and (11) results in Eq. (12)

$$F_{lat} = \frac{D_L}{D_R} + \frac{4l\lambda}{D_R\theta_L}. \tag{12}$$

Note that in Eq. (12), the lateral corrective factor ($F_{\text{lat}}$) is calculated, which expresses the relationship between the deviation angle and the lateral corrective factor by reading the amounts of the total left wheel actual angular displacement, $\theta_L$, and measurement of orientation angle, $\lambda$. Note that the orientation angle is measured according to the measured errors along $x$ and $y$ axes ($\delta x_i$ and $\delta y_i$):

$$\lambda = \frac{1}{n}\sum_{i=1}^{n} \tan^{-1}\left(\delta y_i / \delta x_i\right), \tag{13}$$

where $n$ is the number of trial runs and, $\delta x_i$ and $\delta y_i$ are the longitudinal and lateral errors measured in each trial as shown in Fig. 4. The goal now is to use the lateral corrective factor appropriately to the robot motion equations (to be described in the next section) such that the deviation angle, $\lambda$, converges to zero, i.e., the robot manages to stay along the desired path (path A). However, even if the robot is aligned with the desired path, we need to further ensure that it reaches the desired location, i.e., having no longitudinal error, $\delta x$. This is done by equally adjusting the speeds of the wheels. Thus, a second coefficient, termed longitudinal corrective factor, $F_{lon}$, is defined:

$$F_{\text{lon}} = \frac{L}{\sqrt{(L-\delta x)^2 + (\delta y)^2}}, \tag{14}$$

where $L$ is the length of path, $\delta x = \frac{1}{n}\sum_{i=1}^{n}\delta x_i$, and $\delta y = \frac{1}{n}\sum_{i=1}^{n}\delta y_i$. The significance of the proposed method is that it is built on simple and easy to understand kinematics equations. Additionally, the method does not make any assumption on the sources of error in robot motion.

## 5. Implementation

As described in Sections 3 and 4, the UMBmark method corrects the robot motion using two corrective factors $\alpha$ and $\beta$ while the proposed method compensates for the robot error using lateral and longitudinal corrective factors $F_{\text{lat}}$ and $F_{\text{lon}}$. The most integrated approach to implement these factors in the robot equations of motion is to use them within the Jacobian matrix that relates robot trajectory (position and orientation) variables, $\dot{X}_{3\times1} = [\dot{x}\ \dot{y}\ \dot{\theta}]^T$, to the joint (wheel) variables, $\dot{\Theta}_{2\times1} = [\dot{\theta}_L\ \dot{\theta}_R]^T$. This relation is shown in the following equation, which is obtained by combining Eqs. (1) and (2)

$$\begin{bmatrix}\dot{\theta}_L\\ \dot{\theta}_R\end{bmatrix} = \begin{bmatrix}\frac{2}{D_L}\cos(\theta) & \frac{2}{D_L}\sin(\theta) & -\frac{l}{D_L}\\ \frac{2}{D_R}\cos(\theta) & \frac{2}{D_R}\sin(\theta) & \frac{l}{D_R}\end{bmatrix}\begin{bmatrix}\dot{x}\\ \dot{y}\\ \dot{\theta}\end{bmatrix}. \tag{15}$$

This type of implementation allows one to extend the method to wheeled mobile robots with more than two driving wheels. If there is no positioning error in the robot motion, the

https://doi.org/10.1017/S0263574711001329 Published online by Cambridge University Press

Table I. Specifications of prototype robots.

| | Robot 1 | Robot 2 | Robot 3 | Robot 4 | Robot 5 | Robot 6 |
|---|---|---|---|---|---|---|
| Dimension (L × W × H; cm) | 10 × 10 × 22.5 | 13 × 18 × 20 | 18 × 32 × 14 | 20 × 20 × 18 | 7 × 7 × 11 | 28 × 28 × 9 |
| Weight (kg) | 0.880 | 1.250 | 3.280 | 1.800 | 0.105 | 0.450 |
| Stall torque of motor (nm) | 0.2 | 1.0 | 0.2 | 3.0 | 0.1 | 0.2 |
| Maximum linear speed (m/min) | 0.115 | 0.095 | 0.230 | 0.210 | 0.820 | 0.270 |
| Wheel radius (cm) | 5.0 | 3.5 | 5.5 | 1.3 | 2.5 | 3.5 |
| Wheelbase (cm) | 10.5 | 6.1 | 8.6 | 9.0 | 3.2 | 13.5 |
| Encoder resolution (pulse/rev) | 48 | 48 | 60 | 36 | 60 | 36 |

corrective factors will be $\alpha = 0$ and $\beta = 0$ in the UMBmark method, and $F_{\text{lat}} = 1$ and $F_{\text{lon}} = 1$ in the proposed method. Thus, the nominal values of the diameters and wheelbase are used as shown in Eq. (15). For other situations, Eq. (15) must be expressed as Eq. (16) when using the UMBmark technique, or Eq. (17) when using the proposed method:

$$\begin{bmatrix} \dot{\theta}_L \\ \dot{\theta}_R \end{bmatrix} = \begin{bmatrix} \frac{E_d+1}{D_a}\cos(\theta) & \frac{E_d+1}{D_a}\sin(\theta) & -\frac{E_d+1}{2D_a}E_b l \\ \frac{E_d+1}{D_a E_d}\cos(\theta) & \frac{E_d+1}{D_a E_d}\sin(\theta) & \frac{E_d+1}{2D_a E_d}E_b l \end{bmatrix} \times \begin{bmatrix} \dot{x} \\ \dot{y} \\ \dot{\theta} \end{bmatrix}, \tag{16}$$

$$\begin{bmatrix} \dot{\theta}_L \\ \dot{\theta}_R \end{bmatrix} = \begin{bmatrix} \frac{2F_{\text{Lon}}F_{\text{Lat}}}{D_L}\cos(\theta) & \frac{2F_{\text{Lon}}F_{\text{Lat}}}{D_L}\sin(\theta) & -\frac{F_{\text{Lon}}F_{\text{Lat}}}{D_L}l \\ \frac{2F_{\text{Lon}}}{D_R}\cos(\theta) & \frac{2F_{\text{Lon}}}{D_R}\sin(\theta) & \frac{F_{\text{Lon}}}{D_R}l \end{bmatrix} \times \begin{bmatrix} \dot{x} \\ \dot{y} \\ \dot{\theta} \end{bmatrix}. \tag{17}$$

Note that $E_d$, $E_b$, $F_{\text{lat}}$, and $F_{\text{lon}}$ are determined during the calibration experiments and $D_a = 0.5(D_{R+}D_L)$ denotes the average wheel diameter. Detailed derivations of Eqs. (16) and (17), used for trajectory control of calibrated robots, are given in the Appendix.

## 6. Description of Prototype Robots Used for Evaluation

This section describes all six prototyped mobile robots that were built in-house at different times and with a variety of components to examine the performance of the described benchmark techniques.

Robot 1: *Jumper*

With reference to Fig. 5(a), the Jumper consists of two driving wheels, two stepping motors with gear boxes, two ultrasonic sensors, and a wireless camera to detect the obstacles. This robot is also equipped with a jumping mechanism. This vehicle has been designed to pass over modest obstacles.[21]

Robot 2: *Mobolab*

Mobolab [Fig. 5(b)] has two driving wheels, one free castor wheel, and two stepping motors. Mobolab is programmed to follow trajectories defined by markers on the ground using infrared sensors.

Robot 3: *Robotest*

Robotest [Fig. 5(c)] has two driving wheels activated by stepper motors. The additional two castor wheels provide stability. There are two optical sensors in front of the robot to detect obstacles. This robot is capable of moving in programmed trajectories and detecting obstacles.

Robot 4: *Caterpillar*

As shown in Fig. 5(d), the drive mechanism of Caterpillar consists of two driving wheels, two servo motors with spur gears, and two castor wheels. The wheels are constructed with flexible rubber to create enough friction during the motion.

Robot 5: *Maze*

Maze [Fig. 5(e)] has two driving wheels that are controlled by a microprocessor. The additional castor wheels are to provide better stability. There are two ultrasonic sensors in front of the robot to detect obstacles. This robot has been designed and built for maze competitions.

Robot 6: *Vacuum Cleaner*

The Vacuum Cleaner, shown in Fig. 5(f), works in two self-controlled and remote control modes. This robot has been designed for navigation with high maneuverability on flat and low-friction surfaces. It has four active external sensors, two drive wheels, two castors, and a vacuum system.

Table I shows key specifications of the mobile robots described above.

## 7. Experimental Verification

This section presents results of experimental tests applied to all prototype robots described above. The metric used to facilitate the comparison is the radial error ($\delta r$) as defined below:

$$\delta r = \sqrt{(\delta x)^2 + (\delta y)^2}, \tag{18}$$

where $\delta x$ and $\delta y$ are defined in Figs. 3 and 4 for UMBmark and proposed methods, respectively. The effectiveness of each method is then measured by comparing the mean error improvement index ($\delta r_m$):

$$\delta r_m = [(\delta r_{m,\text{BF}} - \delta r_{m,\text{AF}})/\delta r_{m,\text{BF}}] \times 100\%, \tag{19}$$

where $\delta r_{m,\text{BF}}$ and $\delta r_{m,\text{AF}}$ are the mean values of the radial errors before and after calibration, respectively.

During the experiments, we employed the incremental optical encoders to count the pulses and then determined

https://doi.org/10.1017/S0263574711001329 Published online by Cambridge University Press

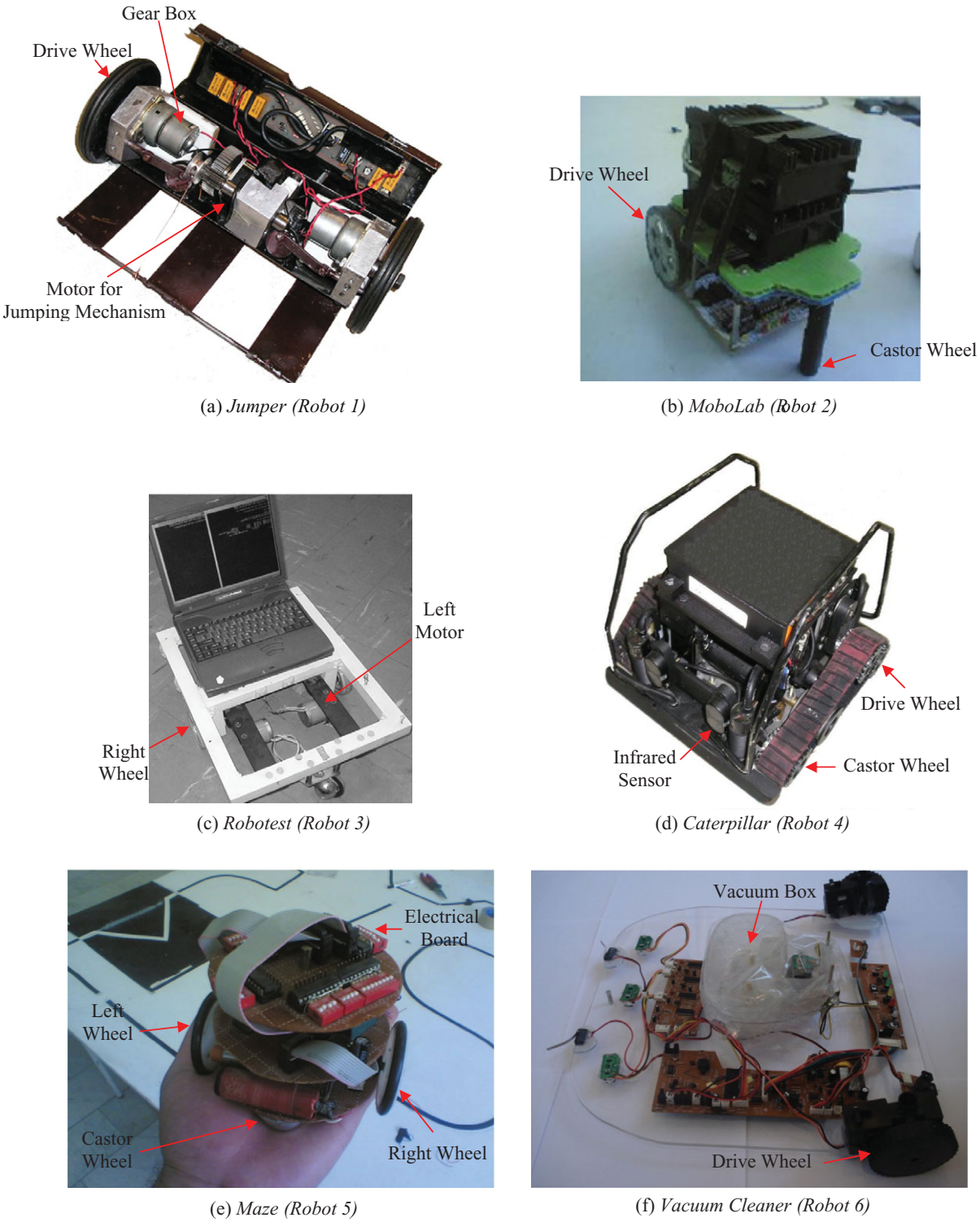


(a) *Jumper (Robot 1)* (b) *MoboLab (Robot 2)*

(c) *Robotest (Robot 3)* (d) *Caterpillar (Robot 4)*

(e) *Maze (Robot 5)* (f) *Vacuum Cleaner (Robot 6)*

Fig. 5. (Colour online) Prototype differential drive mobile robots.

the angular rotation of each wheel:

$$\theta = 2\pi \left(\frac{N}{E}\right). \tag{20}$$

In Eq. (20), $E$ is the resolution of the encoder and $N$ is the number of pulses counted.

Figure 6 shows the position errors before and after calibration using the UMBmark and proposed methods. Note that both the methods were applied to all robots and over many trials. As seen, the motions of all the robots were corrected with either method, i.e., position errors became significantly smaller over the corresponding calibration trajectories. The position errors were measured with respect to the corresponding desired destinations. Note that UMBmark uses square path for calibration, whereas the proposed method moves the robot along a single straight path to calibrate. Consequently, the final desired destinations for each method are not the same (compare Figs. 3 and 4).

https://doi.org/10.1017/S0263574711001329 Published online by Cambridge University Press

Table II. Corrective factors calculated on the basis of calibration experiments.

| | UMBmark method | | Proposed method | | |
|---|---|---|---|---|---|
| | $\alpha$ (rad) | $\beta$ (rad) | $\lambda$ (rad) | $F_{lat}$ | $F_{lon}$ |
| *Robot 1* | −0.19 | 0.31 | 0.09 | 1.020 | 1.024 |
| *Robot 2* | −0.29 | −0.20 | 0.17 | 1.023 | 1.028 |
| *Robot 3* | −0.38 | −0.29 | −0.24 | 1.037 | 0.968 |
| *Robot 4* | 0.41 | 0.31 | −0.02 | 1.033 | 0.966 |
| *Robot 5* | −0.32 | 0.41 | 0.33 | 1.041 | 1.028 |
| *Robot 6* | 0.28 | −.036 | −0.09 | 1.029 | 0.969 |

Table II shows the calculated factors required to correct the robot motion for all robot types. The values of these factors were determined according to the test methods described earlier. As shown in this table, using the proposed method, the values of $F_{lat}$ and $F_{lon}$ vary between 1.020 to 1.041 and 0.966 to 1.028, respectively. $F_{lat}$ is calculated using Eq. (12), where $D_R$, $D_L$, and $l$ are nominal geometrical properties of robots (see Table I). $\theta_L$ is obtained from the encoder counts using Eq. (20). $\lambda$ is determined by measuring positioning errors and employing Eq. (13). Figure 6 confirms that the positioning errors of robot motion were reduced after applying the corrective factors.

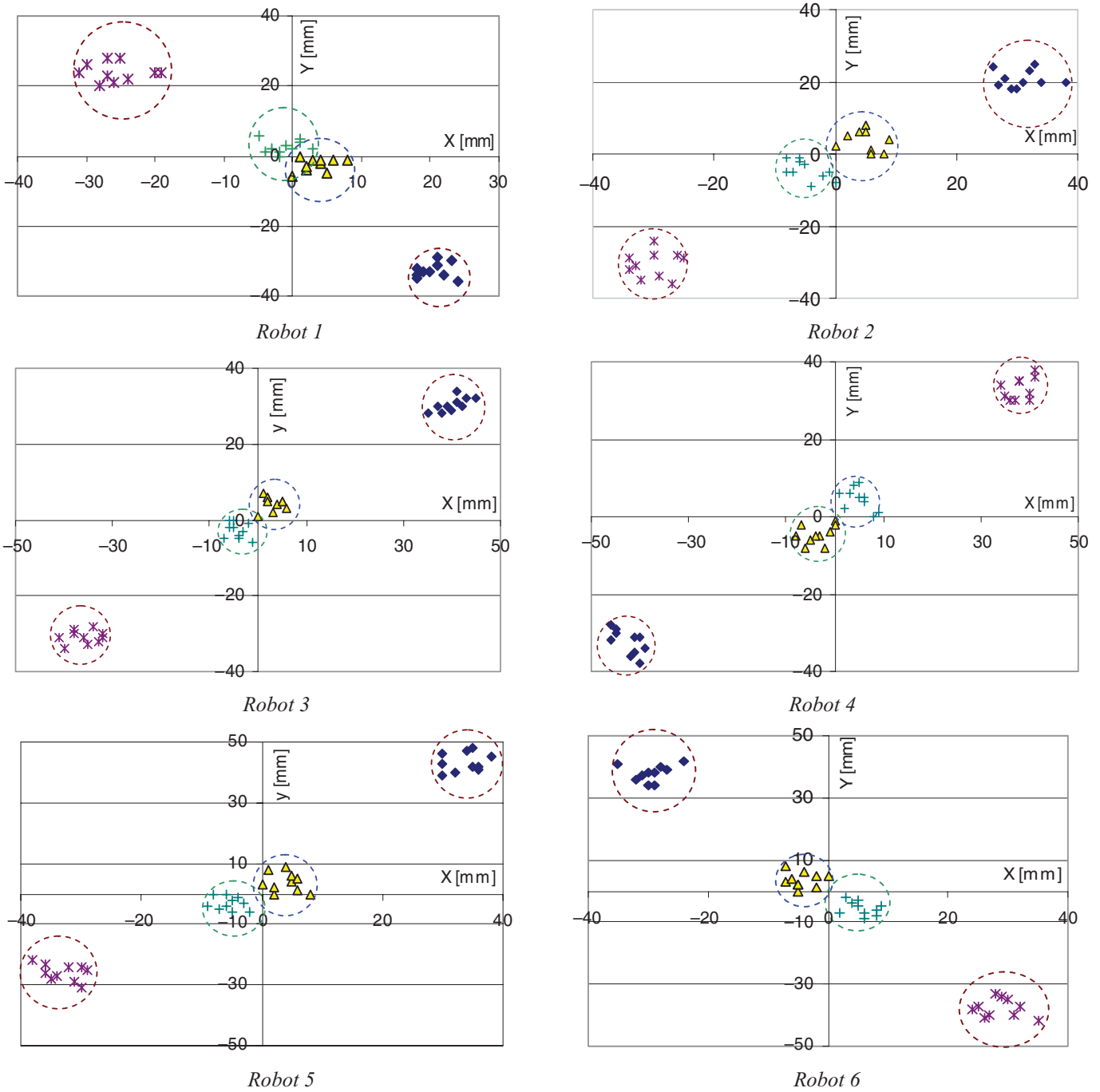


Fig. 6. (Colour online) Positioning errors of six prototype robots: (*i*) UMBmark square calibration path—before calibration (◆) and after calibration (Δ), (*ii*) proposed straight calibration path—before calibration (✳) and after calibration(+).

https://doi.org/10.1017/S0263574711001329 Published online by Cambridge University Press

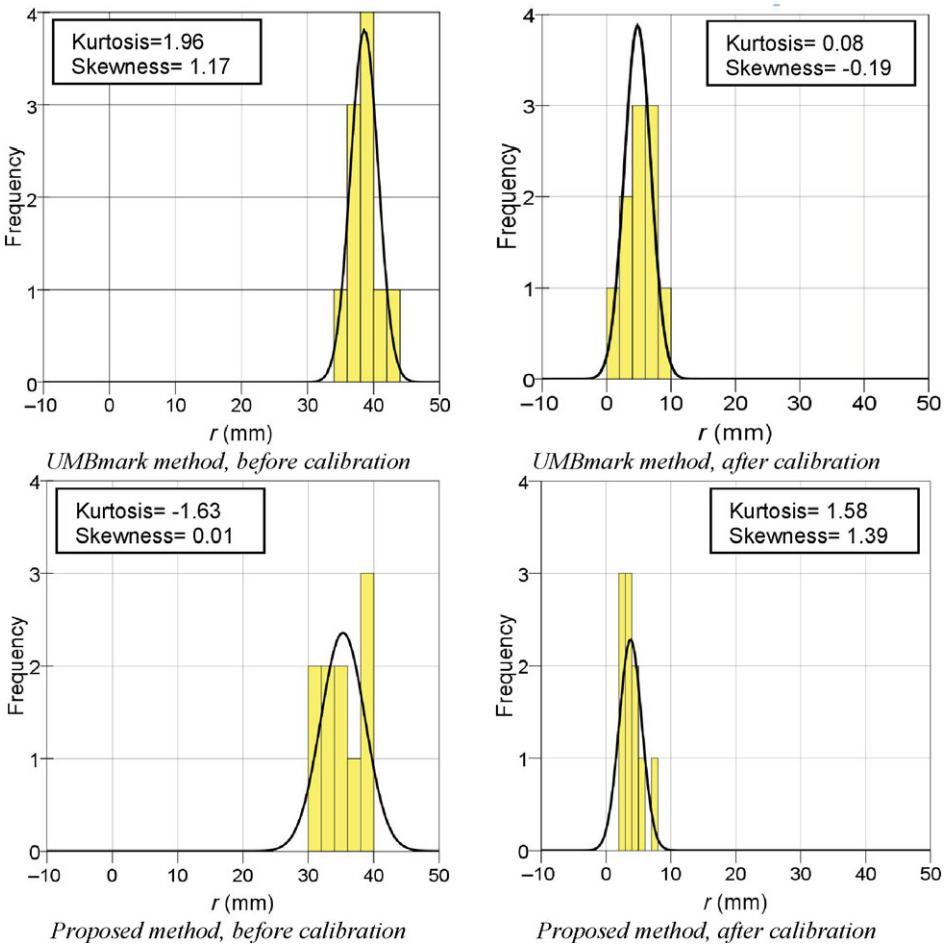


Fig. 7. (Colour online) Normal distribution of accuracy in radial direction (Robot 1). The kurtosis or skewness values of more than 2 indicate that data groups differ or skew to a significant degree.[27]

The form of distribution diagram of position error data, which are derived from experimental tests, is significant to predict the future behavior of robots in motion. One of the most important probability distributions, from both theoretical and practical viewpoints, is the Gaussian (normal) distribution. Figure 7 shows results of benchmark tests for Robot 1. The normal distribution is clearly depicted. The amount of mean, standard deviation, and number of performed tests with this robot can be estimated using these diagrams.

Table III shows values of average errors for all robot types before and after calibration as well as estimates of skewness ($s$), kurtosis ($k$), and standard deviation ($\sigma$) determined from measured data. The fifth column of Table III presents percentage of error improvement ($\delta r_m$). From Table III, it is seen that both methods achieved similar improvements ranging from 80 to 90% and within $\pm 5\%$ difference. Thus, we can claim that the proposed method is comparable to the UMBmark method in terms of the accuracy that can be achieved. Due to the variability of data over many trials, standard deviation is used to measure confidence in statistical conclusions. From Table III, the standard deviation values of all robots before and after calibration can be read. The last two columns show the kurtosis and skewness values of position error data. Kurtosis[26] is the measure of the "peakedness" of the probability distribution of a real-valued random variable. Higher kurtosis means more of the probability distribution of a real-valued random variable.[26]

Note that the kurtosis ($k$) and skewness ($s$) values of the distribution diagrams were calculated using the following equations[28]:

$$k = \frac{\frac{1}{n}\sum_{i=1}^{n}(\delta r_i - \mu)^4}{\left(\frac{1}{n}\sum_{i=1}^{n}(\delta r_i - \mu)^2\right)^2} - 3, \tag{21}$$

$$s = \frac{\frac{1}{n}\sum_{i=1}^{n}(\delta r_i - \mu)^3}{\left(\frac{1}{n}\sum_{i=1}^{n}(\delta r_i - \mu)^2\right)^{1.5}}. \tag{22}$$

Here, $\delta r_i$ denotes the sample value of radial errors and $\mu$ is the corresponding mean value. The calculation of statistical values was done using a sample of 10 from each set of tests ($n = 10$).

The skewness and kurtosis values, illustrated in Table III, confirm that the derived data satisfy the normal distributions criterion. Note that for Robot 4 (R4), the standard kurtosis index is more than 2, which does not satisfy the normality criteria for this state. However, after calibration, this value is reduced to 1.32. Thus, for all conditions, the normality criteria are satisfied which indicates that the test used to measure the trait (positioning error) is good.[29]

https://doi.org/10.1017/S0263574711001329 Published online by Cambridge University Press

Table III. Statistical indices for UMBmark (U) and proposed (P) methods before (BF) and after (AF) calibration.

| | | | Mean ($\mu$) | Improvement ($\delta r_m$; %) | Std. Dev. ($\sigma$) | Kurtosis ($k$) | Skewness ($s$) |
|---|---|---|---|---|---|---|---|
| *Robot 1* | U | BF | 38.6 | 87.57 | 4.40 | 1.96 | 1.17 |
| | U | AF | 4.8 | | 4.23 | 0.08 | −0.19 |
| | P | BF | 35.3 | 89.24 | 11.43 | −1.63 | 0.01 |
| | P | AF | 3.8 | | 3.04 | 1.58 | 1.39 |
| *Robot 2* | U | BF | 37.3 | 80.97 | 11.17 | −1.08 | −0.51 |
| | U | AF | 7.1 | | 5.66 | 1.19 | −0.99 |
| | P | BF | 43.0 | 82.79 | 13.12 | −1.69 | −0.42 |
| | P | AF | 7.4 | | 3.04 | −1.43 | 0.23 |
| *Robot 3* | U | BF | 50.3 | 88.87 | 10.61 | −0.78 | −0.16 |
| | U | AF | 5.6 | | 3.77 | 1.14 | −1.82 |
| | P | BF | 47.4 | 88.19 | 8.62 | −0.58 | 0.47 |
| | P | AF | 5.6 | | 2.68 | 1.13 | −0.38 |
| *Robot 4* | U | BF | 53.6 | 88.43 | 9.11 | −0.91 | −0.42 |
| | U | AF | 6.2 | | 3.22 | −0.63 | −0.63 |
| | P | BF | 51.1 | 85.52 | 21.20 | 3.17 | 1.63 |
| | P | AF | 7.4 | | 4.14 | 1.32 | −1.08 |
| *Robot 5* | U | BF | 54.9 | 88.71 | 10.93 | −0.64 | −0.21 |
| | U | AF | 6.2 | | 7.17 | −1.14 | −0.53 |
| | P | BF | 42.2 | 83.89 | 5.75 | −0.85 | −0.82 |
| | P | AF | 6.8 | | 3.53 | −0.85 | 0.04 |
| *Robot 6* | U | BF | 48.1 | 87.32 | 6.03 | 1.60 | 0.82 |
| | U | AF | 6.1 | | 4.91 | 1.58 | 0.47 |
| | P | BF | 47.5 | 82.95 | 11.90 | −0.80 | −0.51 |
| | P | AF | 8.1 | | 6.72 | −1.08 | −0.38 |

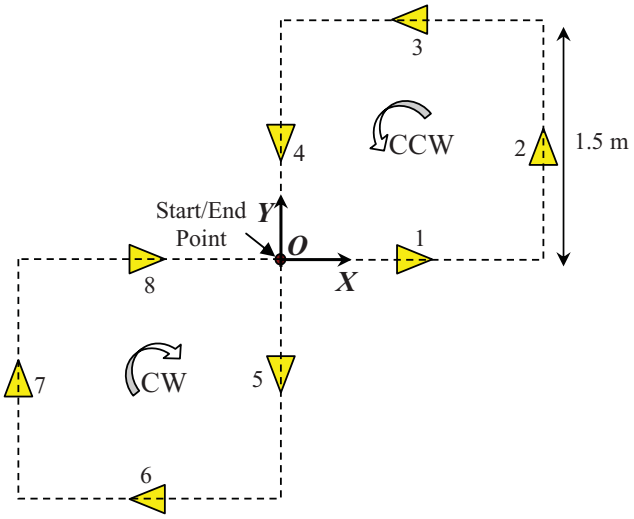


Fig. 8. (Colour online) Unseen path to test the performance of robot calibrated with the UMBmark method or proposed method. Path has been designed to allow the robot to move in a trajectory consisting of straight paths in both CW and CCW directions.

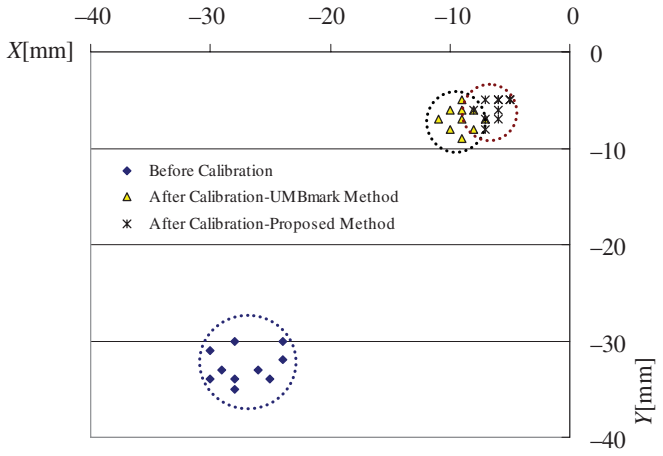


Fig. 9. (Colour online) Positioning of robot before and after calibration.

While the radial error improvements in both the methods are within ± 5% of each other, the experiments showed some advantages in using the proposed method as compared to the UMBmark method. First, the proposed method requires a single straight path for calibration, which is believed to be simpler to implement than the square path needed by the UMBmark technique. The proposed method is also less timely to complete, than the UMBmark method. Specifically, the average time spent to perform full test using the proposed method was approximately 10% of the average time needed to conduct the UMBmark method. Further, since this method is built upon the symbolic form of robot kinematics, it can be extended to calibrate other types of wheeled mobile robots such as omnidirectional mobile robots.

In the next experiment, we programmed one of the calibrated robots (using the two calibration tests outlined earlier) to follow an unseen double square path. This path, which has not been previously used for calibration in either the UMBmark or the proposed method, is used to further compare the workability of the methods. With reference to Fig. 8, the path was designed to move the robot along lines 1 to 8 and return it to the original point "*O*." First, the test was conducted without consideration of corrective factors. Next, the test was repeated on the robot considering the corrective factors obtained by the UMBmark method,

https://doi.org/10.1017/S0263574711001329 Published online by Cambridge University Press

or the proposed method. The experiment was repeated 10 times; Fig. 9 depicts the results. As shown in this figure, the proposed method is slightly better than the UMBmark method. Specifically, the mean error improvement indices for the UMBmark method and the proposed method were 73.18 and 79.62%, respectively.

## 8. Conclusions

Odometry errors in mobile robots with differential drives are inevitable. These errors originate from hard to completely avoid imperfections such as unequal wheels diameters, misalignment at joints, backlash, slippage in encoder pulses, and much more. In this paper, we proposed a method to reduce the odometry errors, and compared its performance with the UMBmark, a commonly used approach in calibration of differential drive mobile robots. The focus was on correcting the systematic errors with an effective, yet simple to implement method. Six prototype differential drive mobile robots were constructed to evaluate the effectiveness of the developed method. Experimental analyses, using the prototype robots, showed that the method can remove odometry errors by 80–90%, which is comparable with the UMBmark method. Further tests using an unseen path showed that a robot calibrated with the proposed method produced slightly less position error than the case whereby it was calibrated with the UMBmark method. The normal distribution diagrams and the values obtained for the skewness and kurtosis indices showed that most of data groups satisfy the normal distribution criterion, especially after calibration, to which both indices were bounded between $-1.82$ and 1.58. Therefore, both calibration methods, which were used to reduce the positioning error of the robot, statistically performed well.

Overall, this paper, which is believed to make a further contribution to the development of sensory systems and techniques for positioning of differential drive mobile robots, showed that the method of calibration in this paper is practical and can lead to positioning improvement in wide applications of mobile robots, and should be seriously considered as a potential method for calibration of mobile robots with differential drive mechanism. Future work should examine the usefulness of this technique toward online calibration to further improve the accuracy of mobile robot motions.

## Appendix

For situations where the values of robot's actual and nominal parameters are not the same, i.e., $\alpha \neq 0$ or $\beta \neq 0$ and, $F_{lat} \neq 1$ or $F_{lon} \neq 1$, the nominal values in Eq. (15) must be replaced with the actual ones, as shown by the following equation:

$$\begin{bmatrix} \dot{\theta}_L \\ \dot{\theta}_R \end{bmatrix} = \begin{bmatrix} \frac{2}{\hat{D}_L}\cos(\theta) & \frac{2}{\hat{D}_L}\sin(\theta) & -\frac{\hat{l}}{\hat{D}_L} \\ \frac{2}{\hat{D}_R}\cos(\theta) & \frac{2}{\hat{D}_R}\sin(\theta) & \frac{\hat{l}}{\hat{D}_R} \end{bmatrix} \begin{bmatrix} \dot{x} \\ \dot{y} \\ \dot{\theta} \end{bmatrix}. \quad \text{(A1)}$$

With reference to Eq. (A1), $\hat{D}_L$ and $\hat{D}_R$ are the actual values of left and right wheel diameters and $\hat{l}$ represents the actual wheelbase of robot. Using the UMBmark method, the relationships between the actual and nominal values of wheelbase as well as wheel diameters are given by Eqs. (8) and (9). By placing Eqs. (8) and (9) into Eq. (A1), the following equation is obtained:

$$\begin{bmatrix} \dot{\theta}_L \\ \dot{\theta}_R \end{bmatrix} = \begin{bmatrix} \frac{2}{\hat{D}_L}\cos(\theta) & \frac{2}{\hat{D}_L}\sin(\theta) & -\frac{E_b l}{\hat{D}_L} \\ \frac{2}{\hat{D}_L E_d}\cos(\theta) & \frac{2}{\hat{D}_L E_d}\sin(\theta) & \frac{E_b l}{\hat{D}_L E_d} \end{bmatrix} \begin{bmatrix} \dot{x} \\ \dot{y} \\ \dot{\theta} \end{bmatrix}. \quad \text{(A2)}$$

From the work by Borenstein,[20] we know that $D_a = 0.5(\hat{D}_R + \hat{D}_L)$. Thus,

$$\frac{1}{\hat{D}_L} = \frac{(\hat{D}_R + \hat{D}_L)/\hat{D}_L}{(\hat{D}_L + \hat{D}_R)} = \frac{\hat{D}_R/\hat{D}_L + 1}{2D_a} = \frac{Ed + 1}{2D_a}. \quad \text{(A3)}$$

Replacing $1/\hat{D}_L$ in Eq. (A2) with its equivalent from Eq. (A3), results in the following relation:

$$\begin{bmatrix} \dot{\theta}_L \\ \dot{\theta}_R \end{bmatrix} = \begin{bmatrix} \frac{E_d+1}{D_a}\cos(\theta) & \frac{E_d+1}{D_a}\sin(\theta) & -\frac{E_d+1}{2D_a}E_b l \\ \frac{E_d+1}{D_a E_d}\cos(\theta) & \frac{E_d+1}{D_a E_d}\sin(\theta) & \frac{E_d+1}{2D_a E_d}E_b l \end{bmatrix} \times \begin{bmatrix} \dot{x} \\ \dot{y} \\ \dot{\theta} \end{bmatrix}. \quad \text{(A4)}$$

Alternatively, for the proposed method, Eq. (A1) can be rewritten using the nominal values of wheel diameters, wheelbase, and the corrective factors, $F_{\text{lat}}$ and $F_{\text{lon}}$. This is done in two stages. First, the angular velocity of the left wheel is adjusted by multiplying it by the lateral corrective factor ($F_{\text{lat}}$). This will ensure that the robot stays along the straight path. The corresponding relationship between the robot trajectory variables and the wheels variables will then become

$$\begin{bmatrix} \dot{\theta}_L \\ \dot{\theta}_R \end{bmatrix} = \begin{bmatrix} F_{\text{Lat}}\left(\frac{2}{D_L}\cos(\theta)\right) & F_{\text{Lat}}\left(\frac{2}{D_L}\sin(\theta)\right) & F_{\text{Lat}}\left(-\frac{1}{D_L}l\right) \\ \frac{2}{D_R}\cos(\theta) & \frac{2}{D_R}\sin(\theta) & \frac{1}{D_R}l \end{bmatrix} \times \begin{bmatrix} \dot{x} \\ \dot{y} \\ \dot{\theta} \end{bmatrix}. \quad \text{(A5)}$$

This modification, although allows the robot to stay on the straight path, does not guarantee that it will reach the final desired destination (point $O$ in Fig. 4). A second modification applied to Eq. (A5) is needed. This modification involves multiplying the entire Jacobian matrix by the longitudinal

https://doi.org/10.1017/S0263574711001329 Published online by Cambridge University Press

corrective factor, $F_{lon}$ and can be expressed as follows:

$$\begin{bmatrix} \dot{\theta}_L \\ \dot{\theta}_R \end{bmatrix} = F_{\text{Lon}} \begin{bmatrix} F_{\text{Lat}}\left(\frac{2}{D_L}\cos(\theta)\right) & F_{\text{Lat}}\left(\frac{2}{D_L}\sin(\theta)\right) & F_{\text{Lat}}\left(-\frac{1}{D_L}l\right) \\ \frac{2}{D_R}\cos(\theta) & \frac{2}{D_R}\sin(\theta) & \frac{1}{D_R}l \end{bmatrix} \times \begin{bmatrix} \dot{x} \\ \dot{y} \\ \dot{\theta} \end{bmatrix}, \tag{A6}$$

or

$$\begin{bmatrix} \dot{\theta}_L \\ \dot{\theta}_R \end{bmatrix} = \begin{bmatrix} \frac{2F_{\text{Lon}}F_{\text{Lat}}}{D_L}\cos(\theta) & \frac{2F_{\text{Lon}}F_{\text{Lat}}}{D_L}\sin(\theta) & -\frac{F_{\text{Lon}}F_{\text{Lat}}}{D_L}l \\ \frac{2F_{\text{Lon}}}{D_R}\cos(\theta) & \frac{2F_{\text{Lon}}}{D_R}\sin(\theta) & \frac{F_{\text{Lon}}}{D_R}l \end{bmatrix} \times \begin{bmatrix} \dot{x} \\ \dot{y} \\ \dot{\theta} \end{bmatrix}. \tag{A7}$$

## References


1. JCGM, "International Vocabulary of Metrology—Basic and General Concepts and Associated Terms," 3rd ed., *JCGM* **200**, 16–34 (2008).
2. C. de Wit, "Trends in Mobile Robot and Vehicle Control," **In**: *Lecture Notes in Control and Information Sciences* (Springer, Berlin, 1998), vol. 230, pp. 151–175.
3. Y. Maddahi and A. Maddahi, "Mobile robots experimental analysis based on kinematics," *WSEAS Trans. Circuits Syst.* **3**, 1662–1667 (2004).
4. K. Jung-Hwan, H. Dong-Choon, J. Yong-Woo and K. Eun-Soo, "Intelligent Mobile Robot System for Path Planning Using Stereo Camera-Based Geometry Information," *Proceedings of the SPIE—The International Society for Optical Engineering*, Boston, USA (Oct. 23, 2005) vol. 6006, pp. 232–243.
5. M. Piaggio, A. Sgorbissa and R. Zaccaria, "Navigation and localization for service mobile robots based on active beacons," *J. Syst. Sci.* **27**(4), 71–83 (2001).
6. B. Bury and J. C. Hope, "Autonomous Mobile Robot Navigation Using a Low-Cost Fibre Optic Gyroscope," *Proceedings of the International Conference on Intelligent Autonomous Vehicles*, Espoo, Finland (June 12–14, 1995) pp. 39–43.
7. W. Kwon, K. S. Roh and H. K. Sung, "Particle Filter-Based Heading Estimation Using Magnetic Compasses for Mobile Robot Navigation," *Proceedings of the 2006 IEEE International Conference on Robotics and Automation*, Orlando, Florida, USA (May 15–19, 2006) pp. 2705–2712.
8. J. Borenstein, "Experimental results from internal odometry error correction with the omnimate mobile robot," *IEEE Trans. Robot. Autom.* **14**(6), 963–969 (1998).
9. G. Antonelli, S. Chiaverini and G. Fusco, "A calibration method for odometry of mobile robots based on the least-square technique: Theory and experimental validation," *IEEE Trans. Robot.* **21**(5), 994–1004 (2005).
10. A. Martinelli and R. Siegwart, "Estimating the Odometry Error of a Mobile Robot During Navigation," *Proceedings of the European Conference on Mobile Robots*, Warsaw, Poland (Sep. 4–6, 2003).
11. N. Roy and S. Thrun, "Online Self-Calibration for Mobile Robots," *Proceedings of the IEEE International Conference on Robotics and Automation*, Detroit, MI, USA (May 10–15, 1999) vol. 3, pp. 2292–2297.
12. S. A. Rahok and O. Koichi, "Odometry Correction with Localization Based on Landmarkless Magnetic Map for Navigation System of Indoor Mobile Robot," *Proceedings of the IEEE International Conference on Autonomous Robots and Agents*, Willington, New Zealand (Feb. 10–12, 2009) pp. 572–577.
13. X. Song and Y. Wang, "A Novel Model-Based Method for Odometry Calculation of All-Terrain Mobile Robots," *Proceedings of the IEEE World Congress on Intelligent Control and Automation*, Chongqing, China (June 25–27, 2008) pp. 581–586.
14. D. Nistér, O. Naroditsky and J. Bergen, "Visual odometry for ground vehicle applications," *J. Field Robot.* **23**(1), 3–20 (2006).
15. P. Marantos, Y. Koveos, L. Stergiopoulos, A. Panousopoulou and A. Tzes, "Mobile Robot Odometry Relying on Data Fusion from RF and Ultrasound Measurements in a Wireless Sensor Framework," *Proceedings of the IEEE Conference on Control and Automation*, Ajaccio, France (June 25–27, 2008) pp. 523–528.
16. E. Papadopoulos and M. Misailidis, "On Differential Drive Robot Odometry with Application to Path Planning," *Proceedings of the European Control Conference*, Kos, Greece (Jul. 2–5, 2007) pp. 5492–5499.
17. F. Chenavier and J. L. Crowley, "Position Estimation for a Mobile Robot Using Vision and Odometry," *Proceedings of the IEEE International Conference on Robotics and Automation*, Nice, France (May 12–14, 1992) pp. 2588–2593.
18. J. Borenstein and L. Feng, "UMBmark: A Benchmark Test for Measuring Dead Reckoning Errors in Mobile Robots," *Proceedings of the SPIE Conference on Mobile Robots*, Philadelphia, PA, USA (Oct. 23–24, 1995) pp. 113–124.
19. J. Borenstein and L. Feng, "UMBmark: A method for measuring, comparing, and correcting dead-reckoning errors in mobile robots," Technical Report, The University of Michigan UM-MEAM-94-22 (1994).
20. J. Borenstein and L. Feng, "Measurement and correction of systematic odometry errors in mobile robots," *IEEE Trans. Intell. Robot. Syst.* **12**(6), 869–880 (1996).
21. Y. Maddahi, M. Seddigh, M. Mohammad Pour and M. Maleki, "Simulation study and laboratory results of two-wheeled mobile robot," *WSEAS Trans. Syst.* **3**, 2807–2812 (2004).
22. Y. Maddahi and A. Maddahi, "YMBM: New method for errors measurements in wheeled mobile robots," *WSEAS Trans. Syst.* **5**, 552–557 (2006).
23. Y. Maddahi, "Design and Laboratory Tests of Wheeled Mobile Robots," *Proceedings of the International Conference on System Science and Simulation in Engineering*, Tenerife, Spain (Dec. 16–18, 2005) pp. 186–191.
24. J. Denavit and R. S. Hartenberg, "A kinematic notation for lower-pair mechanisms based on matrices," *ASME J. Appl. Mech.* **23**, 215–221 (1955).
25. R. Siegwart and I. R. Nourbakhsh, *Introduction to Autonomous Mobile Robots* (Massachusetts Institute of Technology, Cambridge, Massachusetts, USA, 2004) pp. 48–64.
26. K. L. Wuensch, *Encyclopedia of Statistics in Behavioral Science* (Wiley, Chichester, UK, 2005).
27. J. D. Brown, "Statistics corner: Questions and answers about language testing statistics: Skewness and kurtosis," *Shiken: JALT Test. Eval. SIG Newsl.* **1**(1), 20–23 (1997).
28. M. Abramowitz and I. A. Stegun, eds., *Handbook of Mathematical Functions with Formulas, Graphs and Mathematical Tables* (Dover, New York, 1972).
29. Y. P. Aggarwal, *Statistical Methods: Concepts, Application and Computation*, 3rd ed. (Sterling Publishers, New Delhi, 2008).


https://doi.org/10.1017/S0263574711001329 Published online by Cambridge University Press